Quantum Griffiths phase inside the ferromagnetic phase of $Ni_{1-x}V_x$

Ruizhe Wang,[1] Adane Gebretsadik,[1] Sara Ubaid-Kassis,[1,*] Almut Schroeder,[1] Thomas Vojta,[2] Peter J. Baker,[3] Francis L. Pratt,[3] Stephen J. Blundell,[4] Tom Lancaster,[4,†] Isabel Franke,[4] Johannes S. Möller,[4,‡] and Katharine Page[5]

[1] *Physics Department, Kent State University, Kent OH 44242, USA*
[2] *Department of Physics, Missouri University of Science and Technology, Rolla, MO 65409,USA*
[3] *ISIS Facility, STFC Rutherford Appleton Laboratory, Harwell Oxford, Oxfordshire, OX11 0QX, UK*
[4] *Clarendon Laboratory, Department of Physics, Oxford University, Parks Road, Oxford OX1 3PU, UK*
[5] *Spallation Neutron Source, Oak Ridge National Laboratory, Oak Ridge, TN*

(Dated: July 1, 2017)

We study by means of bulk and local probes the d-metal alloy $Ni_{1-x}V_x$ close to the quantum critical concentration, $x_c \approx 11.6\%$, where the ferromagnetic transition temperature vanishes. The magnetization-field curve in the ferromagnetic phase takes an anomalous power-law form with a nonuniversal exponent that is strongly x-dependent and mirrors the behavior in the paramagnetic phase. Muon spin rotation experiments demonstrate inhomogeneous magnetic order and indicate the presence of dynamic fluctuating magnetic clusters. These results provide strong evidence for a quantum Griffiths phase on the ferromagnetic side of the quantum phase transition.

Quantum phase transitions (QPTs) [1] continue to be a central topic in condensed matter physics because they are responsible for a variety of unconventional low-temperature phenomena. For example, the spin fluctuations associated with QPTs between magnetic and nonmagnetic ground states can lead to non-Fermi liquid behavior or even induce novel phases of matter [2].

Real materials always contain some disorder in the form of vacancies, impurities, and other defects. In particular, disorder is unavoidable if the QPT is tuned by varying the composition x in a random alloy such as $Ni_{1-x}Pd_x$, $CePd_{1-x}Rh_x$, or $Sr_{1-x}Ca_xRuO_3$. Research has shown that disorder can dramatically change a QPT and induce a quantum Griffiths phase, a parameter region close to the transition point that is characterized by anomalous thermodynamic behavior. This was established for model Hamiltonians [3, 4] and later predicted to occur in itinerant magnets [5, 6], superconductors [7, 8], and other systems (for reviews see, e.g., Refs. [9]).

Signatures of a magnetic quantum Griffiths phase have been observed, e.g., in diluted Ce compounds [10] and, perhaps most convincingly, in the paramagnetic phase of the d-metal alloy $Ni_{1-x}V_x$ [11, 12]. They consist in anomalous nonuniversal power-law dependencies of the magnetization, susceptibility and other thermodynamic quantities on temperature and magnetic field for concentrations x close to but above the quantum critical concentration x_c (where the ferromagnetic transition temperature is suppressed to zero). These quantum Griffiths singularities can be attributed to rare magnetic regions embedded in the paramagnetic bulk, as predicted in the infinite-randomness scenario for disordered itinerant Heisenberg magnets [6, 7].

Do such Griffiths singularities also exist inside the long-range ordered, ferromagnetic phase? Theoretical arguments [13, 14] suggest that rare isolated magnetic clusters produce anomalous thermodynamic behavior on the ferromagnetic side of the QPT as well as on the paramagnetic side. However, the resulting quantum Griffiths singularities are less universal; depending on the details of the underlying disorder, they range from being stronger than the paramagnetic ones to being much weaker. So far, clear-cut experimental observations of a quantum Griffiths phase inside the long-range ordered phase have been missing [15] (see Ref. [16] for a comprehensive review of QPTs in metallic ferromagnets).

In this Letter, we report the results of magnetic measurements and muon spin rotation (μSR) experiments in $Ni_{1-x}V_x$ across the ferromagnetic QPT. Close to the critical concentration $x_c \approx 11.6\%$, the dependence of the low-temperature magnetization M on the magnetic field H is well described by anomalous power laws on both sides of the transition. On the paramagnetic side, $M \sim H^\alpha$ as in earlier work [11, 12]. On the ferromagnetic side, we observe $M - M_0 \sim H^\alpha$ where M_0 is the spontaneous magnetization. The exponent α is strongly x-dependent (i.e., nonuniversal) and decreases towards zero at x_c. Strikingly, its x-dependence is almost symmetric in $x - x_c$. μSR measures the local magnetic fields inside the sample and reveals the microscopic origins of this anomalous behavior. In the ferromagnetic phase we find a broad distribution of local magnetic fields signifying inhomogeneous magnetic order. μSR data for samples close to x_c also indicate that fluctuating magnetic clusters coexist with the long-range ordered bulk. These results provide strong evidence for a quantum Griffiths phase on the ferromagnetic side of the QPT in $Ni_{1-x}V_x$.

Polycrystalline spherical samples of $Ni_{1-x}V_x$ with $x =$ 0 to 15% were prepared and characterized as described in Refs. [11, 17]. A pair distribution function analysis supports the random distribution of the V atoms. Details of the sample preparation, the characterization with neutron scattering, as well as the magnetization and μSR measurements (performed at PSI and ISIS) are summa-

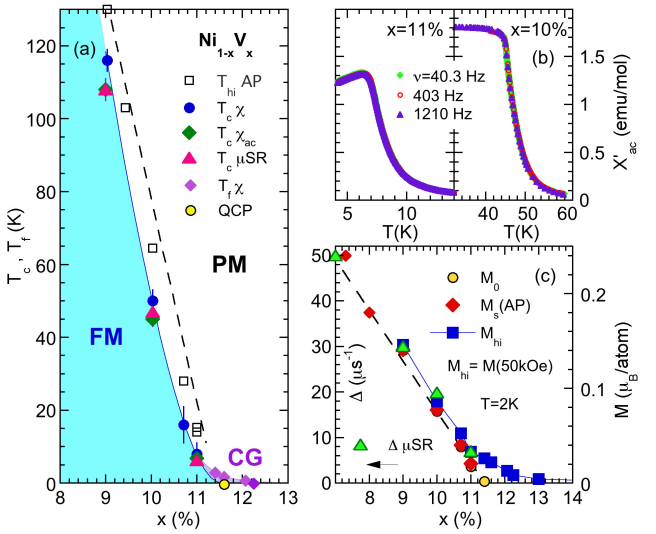

FIG. 1. (a) Phase diagram of $Ni_{1-x}V_x$ showing paramagnetic (PM), ferromagnetic (FM), and cluster glass (CG) phases. The ferromagnetic transition temperature T_c is found using three different methods (see text), leading to a quantum critical point (QCP) at $x_c = 11.6\%$. The high-field (Arrott plot) estimate T_{hi} of the transition shows a linear x-dependence (dashed line). (b) ac-susceptibility χ'_{ac} vs. temperature T (absolute scale estimated by dc-M). T_c is marked by a cusp independent of frequency ν (c) Zero-field moment M_s (from Arrott plots), M_0 (from $M(H)$ power law) and μSR field distribution width Δ show linear x-dependencies (dashed line). M_{hi} is the magnetization in a field of $H = 50\,\mathrm{kOe}$. Data of T_{hi} and M_s from [19, 20] included.

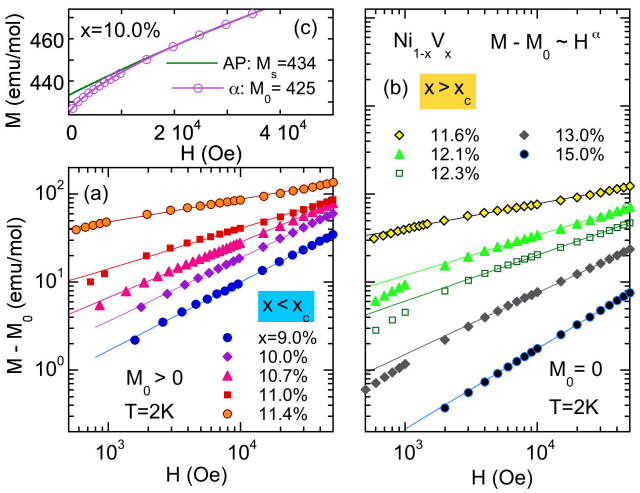

FIG. 2. Magnetization M vs (internal) magnetic field H for several compositions x at the lowest $T = 2\,\mathrm{K}$. An offset $M_0(x) > 0$ has been subtracted for $x < x_c$ in (a); $M_0 = 0$ for $x \geq x_c$ in (b). Solid lines represent fits to $M(H) = M_0 + d_\alpha H^\alpha$. (c) M vs H for $x = 10\%$ with power-law fit defining M_0 and Arrott plot (AP) fit defining M_s.

rized in the Supplemental Material [18].

At first glance, $Ni_{1-x}V_x$ features a simple phase diagram: The ferromagnetic ordering temperature T_c and the spontaneous magnetization M_s are linearly suppressed with increasing x and vanish between $x = 11\%$ and 12%, as shown in Figs. 1(a) and 1(c). This critical concentration is much smaller than the corresponding $x_c = 97.5\%$ for $Ni_{1-x}Pd_x$ [21] because the V atoms, with 5 fewer d-electrons than Ni, also suppress the spins of their Ni neighbors and thus create large defects [22, 23]. The inhomogeneous suppression of magnetic order causes deviations from the linear x-dependence of T_c close to the critical concentration. We determined T_c from the maximum of the susceptibility $dM/dH(T, H \to 0)$ [12], the cusp in the ac susceptibility $\chi'_{ac}(T, H = 0)$ [24] (see Fig. 1(b)), and the onset of the zero-field μSR amplitude $A_{FM}(T)$ [17] (see Fig. 4 below). All estimates agree well with each other. The resulting $T_c(x)$ curve develops a tail and follows the prediction [7] of the infinite-randomness scenario, giving a critical concentration $x_c = 11.6\%$. (In contrast, the tail is absent when an ordering temperature T_{hi} is estimated via extrapolation from high fields, e.g, via standard Arrott plots of H/M vs. M^2.)

The actual quantum critical point at $T = 0$ and $x = x_c$ is masked by a cluster glass phase that appears for $x \gtrsim 11.4\%$ below a freezing temperature $T_f \leq 3\,\mathrm{K}$, see Fig. 1(a) [11, 24]. It is rapidly suppressed by small dc fields and does not affect the physics considered in this Letter.

We now analyze the field dependence of the magnetization M at low T. Figure 2 shows M vs. H at $T = 2\,\mathrm{K}$ for V concentrations x on both sides of the QPT. For paramagnetic samples ($x \geq x_c = 11.6\%$), the magnetization follows the anomalous power law $M(H) = d_\alpha H^\alpha$ over an extended field range from about 2 kOe to the highest available field of 50 kOe. Interestingly, the field dependence of the magnetization in the long-range ordered ferromagnetic phase ($x < x_c$) is also well described by a power-law form, viz., $M(H) = M_0 + d_\alpha H^\alpha$ where M_0 represents the nonzero spontaneous magnetization. As in the paramagnetic phase, these power laws hold in a wide field range from about 1 or 2 kOe to 50 kOe (while the conventional Arrott plot description breaks down below about 10 kOe, see Fig. 2(c)).

The exponent α is nonuniversal, i.e., strongly x-dependent. It has a minimum close to the critical concentration x_c and increases monotonically towards the linear-response value $\alpha = 1$ with increasing distance from x_c, as shown in Fig. 3(b). Strikingly, the $\alpha(x)$ curve is nearly symmetric in $x - x_c$. It can be fitted with a power law, $\alpha(x) \sim |x - x_c|^{\nu\psi}$ with exponent $\nu\psi \approx 0.34 \pm 0.08$ [25] confirming $x_c = 11.6\% \pm 0.1\%$.

What is the origin of these unusual magnetization-field curves? In the paramagnetic phase, they can be attributed to magnetic clusters that are embedded in the paramagnetic bulk [11, 12]. These clusters exist on rare Ni-rich regions in the sample. Their slow independent fluctuations lead to anomalous power laws, the Grif-

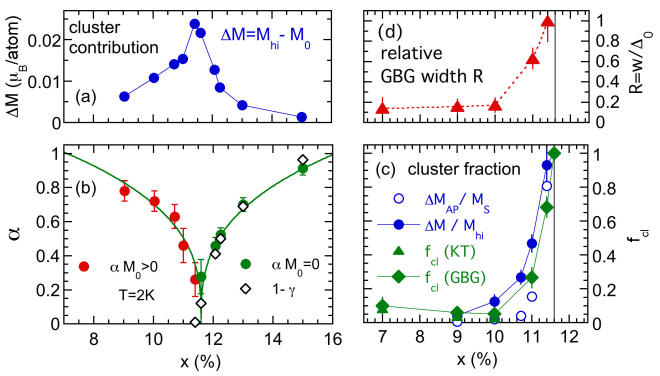

FIG. 3. (a) Cluster contribution $\Delta M = M_{hi} - M_0$ with $M_{hi} = M(50\text{kOe})$ vs. concentration x in $Ni_{1-x}V_x$. (b) Non-universal exponent α vs. x, and susceptibility exponents γ from Ref. [11]. Lines are universal power-law fits $\alpha(x) \sim |x - x_c|^{\nu\psi}$. (c) Cluster fraction f_{cl} vs. x from different methods. (d) Relative width $R = w/\Delta_c$ vs. x of the Gaussian-broadened Gaussian used in the μSR analysis. Data evaluated at lowest temperature ($1.5 - 2\,\text{K}$ for $x > 10\%$).

fiths singularities, in the temperature and field dependencies of various thermodynamic quantities [9]. Deviations at the lowest fields and temperatures stem from weak interactions between the rare regions that freeze their dynamics [11, 26] [27]. Our observation of anomalous magnetization-field curves *below* the critical concentration x_c indicates that disconnected magnetic clusters that fluctuate independently from the long-range ordered bulk also play a crucial role inside the ferromagnetic phase.

To analyze the importance of these clusters quantitatively, we estimate their contribution to the magnetization. A conservative estimate can be obtained by comparing the spontaneous magnetization M_0 with the zero-field magnetization M_s obtained via Arrott plot extrapolation from high fields (see in Fig. 1(c)). As the clusters are disconnected from the bulk, they do not contribute to M_0. In high fields they are fully polarized, however, and thus included in M_s. Consequently, $\Delta M_{AP} = M_s - M_0$ measures the cluster contribution to M. Alternatively, one could simply evaluate $\Delta M = M_{hi} - M_0$ with $M_{hi} = M(H = 50\,\text{kOe})$ and define the cluster fraction as $\Delta M/M_{hi}$ [28]. The x-dependence of ΔM is shown in Fig. 3(a). ΔM has a maximum close to x_c and decreases for $x > x_c$ because the total number of magnetic Ni atoms decreases. ΔM also decreases for $x < x_c$ because it becomes less likely that a magnetic cluster remains disconnected from the bulk. By comparing ΔM with the typical cluster moment of $12\,\mu_B$ [11, 12], we estimate a cluster density at x_c of about one cluster per 500 Ni atoms. Figure 3(c) presents the cluster fractions $\Delta M_{AP}/M_s$ and $\Delta M/M_{hi}$ as functions of x. The measures track each other and indicate that clusters become relevant for $x > 10\%$.

To gain microscopic insight into these clusters and their dynamics, we employ μSR experiments (see, e.g., Ref. [29] for an introduction and Ref. [30] for a technical review). In this technique, spin-polarized positive muons are implanted in the sample. Their spins then precess in the local magnetic field at the stopping site until the muon decays, with a positron emitted preferentially in the direction of the muon spin. Analyzing the asymmetry $A(t)$ of the positron emission as a function of time thus gives direct access to the distribution of *local* magnetic fields in the sample. μSR played an important role in characterizing unconventional magnetism, e.g., in heavy-fermion compounds [31], spin glasses [32], and disordered, non-Fermi liquid metals [33]. As μSR experiments are sensitive towards small magnetic moments, spatial inhomogeneities, and slow fluctuations, they are well suited to identify and study magnetic clusters.

Data for the muon asymmetry $A(t)$ in zero magnetic field for several samples from $x = 0$ to 12.3% are presented in the Supplemental Material [18], together with further details of the analysis. For pure Ni ($x = 0$), $A(t)$ features a single (nearly undamped) precession frequency confirming a uniform local magnetic field and thus uniform ferromagnetic order. In contrast, the $x = 12.3\%$ sample on the paramagnetic side of the QPT shows a very weak depolarization. It can be described by a simple exponential decay, $A(t) = A_{PM}P_{PM}(t) = A_{PM}\exp(-\lambda t)$, caused by quasistatic diluted V nuclear spins as well as by fluctuating Ni clusters in the extreme motional narrowing limit.

Here, we focus on two samples ($x = 10\%$ and 11%) that are close to the QPT but on its ferromagnetic side. At low temperatures, $A(t)$ of the $x = 10\%$ sample (shown in Fig. 4(a)) features a single dip but no further oscillations. Analogous behavior is observed for $7\% \le x \le 10\%$ [17]. It can be described by a Gaussian distribution of local magnetic fields of width Δ, leading to $A(t) = A_{FM}P_{FM}(t)$ with $P_{FM}(t) = P_{KT}(t;\Delta)$ where $P_{KT}(t;\Delta)$ is the well-known Kubo-Toyabe (KT) depolarization function [34]. At temperatures below about $0.5\,T_c$, the data follow the static KT form, signifying a moderately inhomogeneous, long-range ordered state.

Over the entire temperature range, $A(t)$ can be modeled by two components (with temperature-dependent amplitudes) and a small constant background term,

$$A(t) = A_{PM}(T)P_{PM}(t) + A_{FM}(T)P_{FM}(t) + A_{BG} \ . \quad (1)$$

The temperature dependence of the relative amplitude $f_{FM} = A_{FM}/(A_{FM} + A_{PM})$ which represents the FM fraction of the sample is presented in Fig. 4(c). It rapidly increases as the temperature is lowered below T_c and reaches values close to unity for $T \le 0.7\,T_c$. The width Δ of the local magnetic field distribution increases with decreasing T; below about $0.7\,T_c$, $\Delta \propto M_0$ as shown in Fig. 4(d).

For $x = 11\%$, the KT form fails to describe $A(t)$ (shown in Fig. 4(d)) as the typical dip is missing; data taken

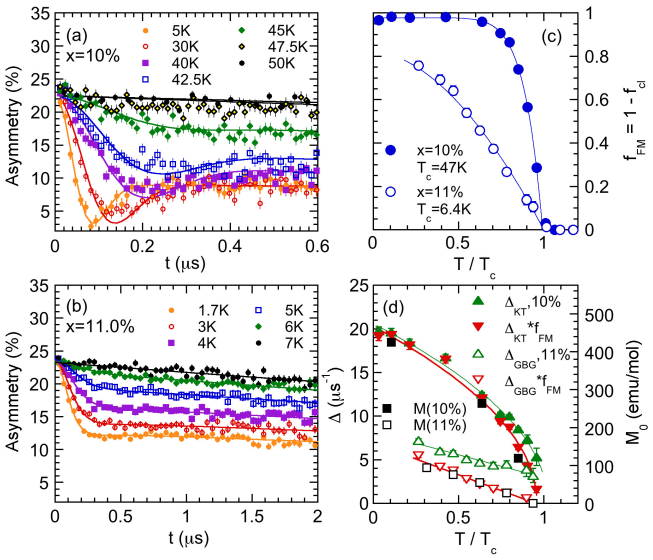

FIG. 4. (a,b) μSR asymmetry A vs. time t for different concentrations x and temperatures T (collected at DOLLY, SμS). Lines represent fits to Eq. (1) using different $P_{FM}(t)$: KT form for $x = 10\%$ (a), GBG form for $x = 11\%$ (b), (for details see text). (c) ferromagnetic fraction (amplitude ratio) f_{FM} vs. temperature T. (d) Field distribution width $\Delta = \Delta_{KT}$ for $x = 10\%$ and $\Delta = \Delta_{GBG}$ for $x = 11\%$ in frequency units $\Delta = \gamma_\mu \langle B_{loc}^2 \rangle^{1/2}$ (with $\gamma_\mu = 2\pi \times 135.5\,\mathrm{MHz/T}$). The magnetization M_0 and Δ are proportional to each other (with $M_0/\Delta \approx 23\,\mathrm{emu/mol\,MHz}$), but only if Δ is scaled by f_{FM}.

in longitudinal fields also exclude a dynamic KT form [17]. A nearly static broader-than-Gaussian field distribution can account for the main, fast time dependence of $A(t)$. In fact, $A(t)$ can be fitted well using Eq. (1) with $P_{FM} = P_{GBG}(t; \Delta_0, w)$ where P_{GBG} is the static "Gaussian-broadened Gaussian" (GBG) depolarization function suggested in Ref. [35], and Δ_0 and w are the average and width of the Gaussian of Gaussians. The temperature dependencies of the effective distribution width $\Delta_{GBG} = (\Delta_0^2 + w^2)^{1/2}$ and of the relative amplitude f_{FM} are shown in Figs. 4(d) and (c). The need for a broad field distribution to describe the ferromagnetic component indicates strongly inhomogeneous order. Moreover, the ferromagnetic ratio f_{FM} increases only slowly below T_c, and a sizable paramagnetic contribution representing about 20% of the sample volume remains even at the lowest T. This paramagnetic contribution stems from the fluctuating moments of Ni-rich clusters that are disconnected from the long-range ordered bulk.

The cluster fraction $f_{cl} = 1 - f_{FM}$ can be obtained for all x using KT and GBG fits of $A(t)$ at the lowest T. As shown in Fig. 3(c), these μSR based cluster fractions agree well with the estimates from the magnetization data and indicate that clusters are relevant for $x > 10\%$. Accordingly, the relative width $R = w/\Delta_0$ of the Gaussian of Gaussians [35] in the field distribution starts increasing for $x > 10\%$, as shown in Fig. 3(d).

In summary, we studied the d-metal alloy $Ni_{1-x}V_x$ close to its quantum-critical concentration x_c, focusing on the ferromagnetic side of the QPT. We found that the low-temperature magnetization-field curve in the ferromagnetic phase follows the power-law $M(H) = M_0 + d_\alpha H^\alpha$ in analogy to the power-law Griffiths singularity $M(H) \sim H^\alpha$ on the paramagnetic side. This anomalous behavior can be attributed to magnetic clusters existing on disconnected rare Ni-rich regions of the sample. Further evidence for such clusters comes from μSR experiments that reveal strongly inhomogeneous magnetic order and the presence of paramagnetic, fluctuating moments inside the long-range ordered ferromagnet (for samples sufficiently close to x_c). These results provide evidence for a quantum Griffiths phase inside the ferromagnetic phase and demonstrate that QPTs in strongly disordered systems are qualitatively different not just from their clean counterparts but also from disordered classical phase transitions. Disorder at a classical transition may change its universality class or turn a first-order transition continuous. In contrast, we observed much stronger effects. Thermodynamic and other properties of $Ni_{1-x}V_x$ close to its QPT are dominated by rare events, resulting, for example, in a diverging magnetic susceptibility not just at x_c but over a range of x close to x_c.

In theoretical studies of model Hamiltonians [13, 14], quantum Griffiths phases on the magnetic side of the QPT are much less universal than those on the paramagnetic side. This stems from the fact that the probability of finding a magnetic cluster that is disconnected from the long-range ordered bulk of the system depends on the details of the disorder. Specifically, in a percolation scenario, a magnetic cluster can be isolated by a surface (shell) of nonmagnetic sites (or broken bonds). Such events have a comparatively high probability; the resulting Griffiths singularities on the ferromagnetic side are thus expected to be stronger than power laws, i.e., stronger than their paramagnetic analogs [13]. For weak disorder, in contrast, a cluster has be far away from the long-range ordered bulk to be isolated. This reduces the cluster probability and leads to ferromagnetic Griffiths singularities that are weaker than the power laws on the paramagnetic side [14]. The disorder in $Ni_{1-x}V_x$ is not purely percolational because the material is a metal, but it is rather strong because each V atom creates a large local defect. The strength of the quantum Griffiths singularities is therefore expected to be between the above limiting cases, in agreement with our observations. However, the existing theories cannot explain the striking symmetry in $x - x_c$ of the Griffiths singularities found here [36]. This remains a challenge for future work.

This work was supported by the NSF under Grant No. DMR-1506152 and by EPSRC (UK). We are grateful for the provision of beam time at the STFC ISIS Muon Facility and SμS, Paul Scherrer Institut, Switzerland. This

work has benefitted from the use of NPDF at the Los Alamos Neutron Science Center, Los Alamos National Laboratory, funded by the US Department of Energy. Part of this research was conducted at the NOMAD instrument at the Spallation Neutron Source, a US Department of Energy Office of Science User Facility operated by Oak Ridge National Laboratory.

* Present address: Sonoma State University, Department of Engineering Science, Rohnert Park, CA 94928
† Present address: Durham University, Centre for Materials Physics, South Road, Durham DH1 3LE, UK
‡ Present address: Neutron Scattering and Magnetism, Laboratory for Solid State Physics, ETH Zürich, CH-8093 Zürich, CH

[1] S. Sachdev, Physics World **12**, 33 (1999).
[2] H. von Löhneysen, A. Rosch, M. Vojta, and P. Wölfle, Rev. Mod. Phys. **79**, 1015 (2007).
[3] D. S. Fisher, Phys. Rev. Lett. **69**, 534 (1992); Phys. Rev. B **51**, 6411 (1995).
[4] M. Thill and D. A. Huse, Physica A **214**, 321 (1995).
[5] A. H. Castro Neto and B. A. Jones, Phys. Rev. B **62**, 14975 (2000).
[6] T. Vojta and J. Schmalian, Phys. Rev. B **72**, 045438 (2005).
[7] J. A. Hoyos, C. Kotabage, and T. Vojta, Phys. Rev. Lett. **99**, 230601 (2007); T. Vojta, C. Kotabage, and J. A. Hoyos, Phys. Rev. B **79**, 024401 (2009).
[8] A. Del Maestro, B. Rosenow, M. Müller, and S. Sachdev, Phys. Rev. Lett. **101**, 035701 (2008).
[9] T. Vojta, J. Phys. A **39**, R143 (2006); J. Low Temp. Phys. **161**, 299 (2010).
[10] J. G. Sereni, T. Westerkamp, R. Küchler, N. Caroca-Canales, P. Gegenwart, and C. Geibel, Phys. Rev. B **75**, 024432 (2007); T. Westerkamp, M. Deppe, R. Küchler, M. Brando, C. Geibel, P. Gegenwart, A. P. Pikul, and F. Steglich, Phys. Rev. Lett. **102**, 206404 (2009).
[11] S. Ubaid-Kassis, T. Vojta, and A. Schroeder, Phys. Rev. Lett. **104**, 066402 (2010).
[12] A. Schroeder, S. Ubaid-Kassis, and T. Vojta, J. Phys. Condens. Matter **23**, 094205 (2011).
[13] T. Senthil and S. Sachdev, Phys. Rev. Lett. **77**, 5292 (1996).
[14] O. Motrunich, S. C. Mau, D. A. Huse, and D. S. Fisher, Phys. Rev. B **61**, 1160 (2000).
[15] Unusual scaling behavior in the ferromagnetic phase of $URu_{2-x}Re_xSi_2$ was initially suggested to stem from a Griffiths phase but later work showed that this is likely not the case [37, 38].
[16] M. Brando, D. Belitz, F. M. Grosche, and T. R. Kirkpatrick, Rev. Mod. Phys. **88**, 025006 (2016).
[17] A. Schroeder, R. Wang, P. J. Baker, F. L. Pratt, S. J. Blundell, T. Lancaster, I. Franke, and J. S. Möller, J. Phys. Conf. Series **551**, 012003 (2014).
[18] See Supplemental Material in XXX with Refs. [39–46] for details on sample preparation, experiments and μSR analysis.
[19] F. Bölling, Phys. Kondens. Mater. **7**, 162 (1968).
[20] I. P. Gregory and D. E. Moody, J. Phys. F: Met. Phys. **5**, 36 (1975).
[21] M. Nicklas, M. Brando, G. Knebel, F. Mayr, W. Trinkl, and A. Loidl, Phys. Rev. Lett. **82**, 4268 (1999).
[22] J. Friedel, Nuovo Cimento **7**, 287 (1958).
[23] M. F. Collins and G. G. Low, Proceedings of the Physical Society **86**, 535 (1965).
[24] R. Wang, S. Ubaid-Kassis, A. Schroeder, P. Baker, F. Pratt, S. Blundell, T. Lancaster, I. Franke, J. Möller, and T. Vojta, J. Phys. Conf. Series **592**, 012089 (2015).
[25] This estimate of $\nu\psi$ is somewhat smaller than the value $\nu\psi = 0.42$ obtained in Ref. [11] from the x-dependence of the susceptibility exponent γ. The deviation is within the error bars.
[26] V. Dobrosavljevic and E. Miranda, Phys. Rev. Lett. **94**, 187203 (2005).
[27] If the relevant rare regions are so large that order parameter conservation hampers the dynamics of the clusters, the functional form of the Griffiths singularities changes [47]. Based on a typical cluster moment of about $12\,\mu_B$ at x_c [11, 12], this likely does not play a role here.
[28] This measure somewhat overestimates the cluster contribution because M_{hi} in $H = 50$ kOe also contains the bulk response to the field.
[29] S. J. Blundell, Contemporary Physics **40**, 175 (1999).
[30] A. Yaouanc and P. Dalmas de Reotier, *Muon Spin Rotation, Relaxation, and Resonance: Applications to Condensed Matter* (Oxford University Press, Oxford, 2011).
[31] A. Amato, Rev. Mod. Phys. **69**, 1119 (1997).
[32] Y. J. Uemura, T. Yamazaki, D. R. Harshman, M. Senba, and E. J. Ansaldo, Phys. Rev. B **31**, 546 (1985).
[33] D. E. MacLaughlin, R. H. Heffner, O. O. Bernal, K. Ishida, J. E. Sonier, G. J. Nieuwenhuys, M. B. Maple, and G. R. Stewart, J. Phys. Condens. Matter **16**, S4479 (2004).
[34] R. S. Hayano, Y. J. Uemura, J. Imazato, N. Nishida, T. Yamazaki, and R. Kubo, Phys. Rev. B **20**, 850 (1979).
[35] D. R. Noakes and G. M. Kalvius, Phys. Rev. B **56**, 2352 (1997).
[36] Such a symmetry does occur in certain one-dimensional random spin chains [3], but it does not generalize to higher dimensions.
[37] E. D. Bauer, V. S. Zapf, P.-C. Ho, N. P. Butch, E. J. Freeman, C. Sirvent, and M. B. Maple, Phys. Rev. Lett. **94**, 046401 (2005).
[38] N. P. Butch and M. B. Maple, Phys. Rev. Lett. **103**, 076404 (2009).
[39] A. Gebretsadik, R. Wang, A. Schroeder, and K. Page, To be published.
[40] T. Proffen, T. Egami, S. Billinge, A. Cheetham, D. Louca, and J. Parise, Appl. Phys. A **74**, s163 (2002).
[41] J. Neuefeind, M. Feygenson, J. Carruth, R. Hoffmann, and K. K. Chipley, Nuclear Instruments and Methods in Physics Research B **287**, 68 (2012).
[42] T. Proffen and S. J. L. Billinge, J. Appl. Crystallogr. **32**, 572 (1999); C. L. Farrow, P. Juhas, J. W. Liu, D. Bryndin, E. S. Bozin, J. Bloch, T. Proffen, and S. J. L. Billinge, J. Phys. Condens. Matter **19**, 335219 (2007).
[43] T. Proffen, V. Petkov, S. J. L. Billinge, and T. Vogt, Zeitschrift für Kristallographie - Crystalline Materials **217**, 47 (2009).
[44] J. Liu, A. Huq, Z. Moorhead-Rosenberg, A. Manthiram, and K. Page, Chemistry of Materials **28**, 6817 (2016).
[45] E. Kornilov and V. Pomjakushin, Physics Letters A **153**, 364 (1991).

[46] F. Pratt, Physica B **289-290**, 710 (2000).
[47] D. Nozadze and T. Vojta, Phys. Rev. B **85**, 174202 (2012).

Supplemental material for Quantum Griffiths phase inside the ferromagnetic phase of $Ni_{1-x}V_x$

S1. SAMPLE PREPARATION AND EXPERIMENTAL PROCEDURES

Polycrystalline spherical samples of $Ni_{1-x}V_x$ with V concentrations $x = 0$ to 15% were prepared by arc melting from high purity elements (Ni 99.995%, Ni^{58} 99.9%, V 99.8%), annealed at 900 - 1050°C for 3 days, cooled rapidly (> 200°C/min) and characterized as described in Refs. [S1, S2].

Magnetization and ac-susceptibility were measured in a Quantum Design SQUID magnetometer and in an Oxford ^{3}He/^{4}He dilution or ^{4}He cryostat equipped with a pickup coil. A small orbital contribution has been subtracted from the magnetization as explained in [S1], and all data (except the ac susceptibility) are demagnetized displaying the internal field H.

Muon spin rotation (μSR) data were collected at the DOLLY instrument at Swiss Muon Source (SμS), Paul Scherrer Institut and at the MuSR instrument at the ISIS facility using 7-30 pellets of each composition wrapped in silver foil. All samples were measured at DOLLY in a similar Ag-mount, the compound $x = 12.3\%$ was also investigated in different cryostats at MuSR. The asymmetry is shown for the DOLLY data, the other data (with different background) are corrected to match.

To probe the structure and chemical distribution, neutron diffraction data of the same samples were collected [S3] at the NPDF instrument [S4] at the Los Alamos Neutron Science Center and at the NOMAD instrument [S5] at the Spallation Neutron Source. A detailed pair distribution function analysis (using PDFgui [S6]) does not reveal any deviations from a FCC-lattice with random occupancy of V atoms, the fit quality for $x = 15\%$ is as high as in pure Ni. PDF data is known to be sensitive to presence and length-scale of chemical short range order [S7, S8]. While simulated neutron PDF patterns of several V aggregate models confirm a weak sensitivity to the presence of V, V-cluster model fits [S3] to experimental data were found inferior to random occupancy model fits. The lattice constant and the average atomic displacements increase with x as expected due to the larger V-radius ($r_V/r_{Ni} \approx 1.05$)[S3].

S2. RAW DATA AND DETAILS OF THE MUON SPIN ROTATION ANALYSIS

The muon asymmetries $A(t)$ in zero magnetic field for samples having compositions $x = 0$, 4%, 10%, 11%, and 12.3% are shown in Figs. S1 and S2. We model these data over the entire composition and temperature range by a superposition of a ferromagnetic component with amplitude A_{FM}, a paramagnetic component with amplitude A_{PM} and a small constant background A_{BG},

$$A(t) = A_{FM}(T)P_{FM} + A_{PM}(T)P_{PM} + A_{BG} \ . \quad \text{(S1)}$$

A_{BG} is mainly due to the silver mount and was about 2% for all $Ni_{1-x}V_x$ samples (measured in DOLLY instrument). The paramagnetic component is well described by simple exponential decay,

$$P_{PM} = P_{exp} = exp(-\lambda t). \quad \text{(S2)}$$

It is dominated by the quasistatic nuclear V-spins and also contains the effects of fluctuating Ni magnetic clusters. For the nuclear spins, the exponential decay can be understood as the short term limit of a Lorentzian Kubo-Toyabe form appropriate for the diluted V atoms. The fluctuations of Ni magnetic clusters are expected to be fast in this d-metal system with high $T_c(x = 0) = 630\,\mathrm{K}$. The average decay rate λ is thus very small and well in the motional narrowing regime.

The ferromagnetic component is modeled by different functional forms depending on the composition x (see e.g. overview in Ref. [S2]). For $x = 0$ and 4%, we use a generalized Kubo-Toyabe [S9] form P_{genKT} [S10, S11],

$$P_{genKT} = \frac{1}{3} + \frac{2}{3}\exp(-\frac{\Delta^2 t^2}{2})[\cos(\omega t) - \frac{\Delta^2 t}{\omega}\sin(\omega t)] \ . \quad \text{(S3)}$$

It corresponds to a Gaussian distribution of the local magnetic fields with a nonzero mean $H_0 = \omega/\gamma_\mu \neq 0$ and width $\Delta H = \Delta/\gamma_\mu$ with $\gamma_\mu = 2\pi \times 135.5\,\mathrm{MHz/T}$. If $\Delta = 0$, this function reduces to a simple undamped oscillation indicating a homogeneous field (at the same stopping site) in a uniform ferromagnet, as observed for $x = 0$. For $x = 7 - 10\%$, we use a static Kubo-Toyabe (KT) [S9] function

$$P_{KT}(t; \Delta, \nu = 0) = \frac{1}{3} + \frac{2}{3}(1 - \Delta^2 t^2)\exp(-\frac{1}{2}\Delta^2 t^2) \quad \text{(S4)}$$

at low temperatures. It indicates a Gaussian distribution of local fields with negligible mean and width $\Delta H = \Delta/\gamma_\mu$. At temperatures closer to T_c, a dynamic KT form with a finite fluctuation rate ν provides a better fit (using the WIMDA program [S12]).

The KT form works well for x up to 10% but fails for $x \geq 11.0\%$. (Note that longitudinal-field data do not support a dynamic KT form for these samples [S2].) A better description for $x = 11\%$ is achieved by using a broader static field distribution. A Gaussian broadened Gaussian (GBG) is the superposition of multiple Gaussians whose widths themselves are Gaussian distributed with mean Δ_0 and width w. It takes the form [S13]

$$P_{GBG} = \frac{1}{3} + \frac{2}{3}(\frac{1 + R^2}{N})^{3/2}(1 - \frac{\Delta^2 t^2}{N}\exp(-\frac{\Delta^2 t^2}{2N}) \quad \text{(S5)}$$

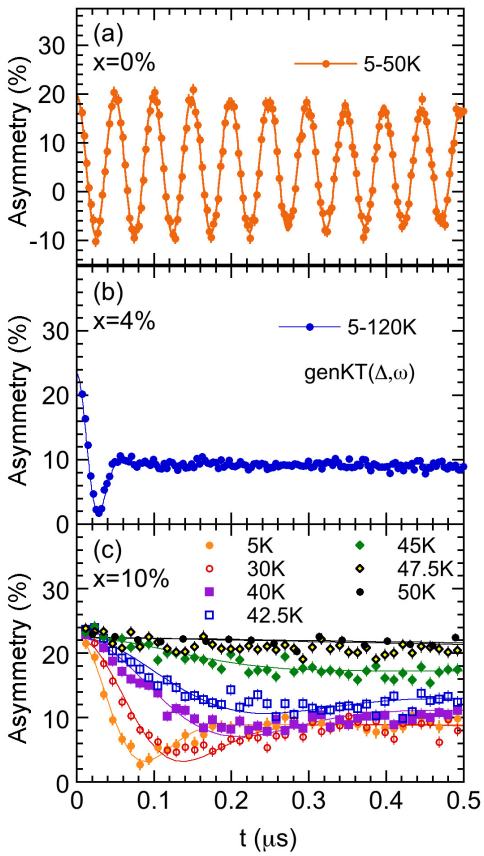

FIG. S1. Zero-field μSR asymmetry A vs. time t of $Ni_{1-x}V_x$. (a) for $x = 0$, (b) for $x = 4\%$ and (c) for $x = 10\%$ at low temperatures T. Lines represent fits to Eq. (S1) with $P_{FM} = P_{genKT}$ for $x = 0\%, 4\%$ and with $P_{FM} = P_{KT}$ for $x = 10\%$. Parameters shown in Fig. S3 and in Fig. S4

with $N = 1+R^2+R^2\Delta^2t^2$, where $R = w/\Delta_0$ is a relative distribution width and $\Delta^2 = \Delta^2_{GBG} = \Delta^2_0 + w^2$ is the square of the recorded effective width. To account for dynamics, the longitudinal term was multiplied by an exponential giving

$$P_{GBG}(t;\nu) = P_{GBG}(t;\nu = 0) + \frac{1}{3}(\exp(-\frac{2}{3}\nu t) - 1) \quad \text{(S6)}$$

where ν is the fluctuation rate of the field.

The evolution of the mean and width of the local-field distribution with x at low temperatures is shown in Fig. S3. The average field ω/γ_μ decreases rapidly with x as the probability of large domains is reduced beyond $x_c/2$, while the width Δ/γ_μ shows a maximum at about $x_c/2$. An effective field $\sqrt{\Delta^2+\omega^2}/\gamma_\mu$ is linearly suppressed with x and can be scaled directly to the mean magnetic moment $m_s(x)$ [S2].

Figure S4 shows additional μSR details for the samples analyzed in the main text, $x = 10\%$ and 11%. For $x = 10\%$, a single Gaussian ($R = 0$) is sufficient to represent the local field distribution. Its width Δ vanishes at

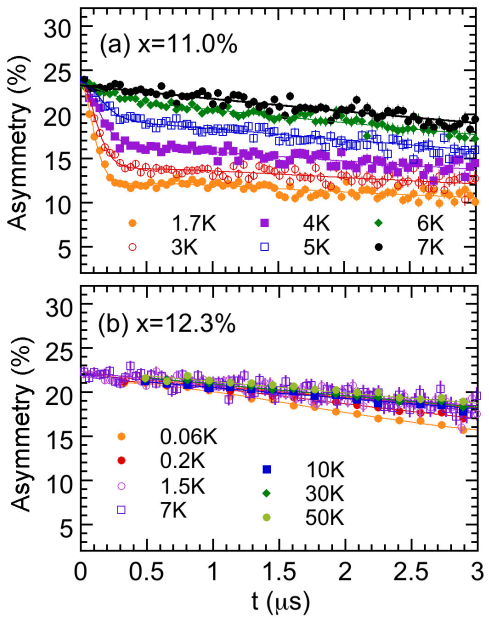

FIG. S2. Zero-field μSR asymmetry A vs. time t for different concentrations x and temperatures T. (a) $A(t)$ for $x = 11.0\%$. Lines represent fits to Eq. (S1) with $P_{FM} = P_{GBG}$. Parameters shown in Fig. S4. (b) $A(t)$ for $x = 12.3\%$. Lines follow P_{PM}.

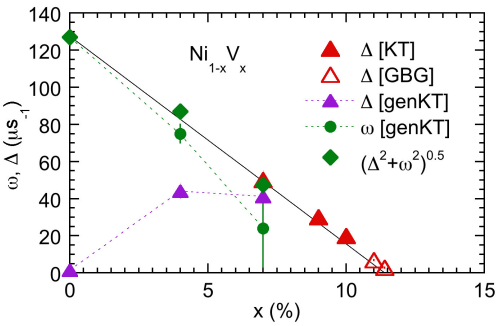

FIG. S3. Energy scales characterizing the local field distribution for various P_{FM} models vs. V-concentration x

T_c, defined by the vanishing of A_{FM} (which matches T_c determined from thermodynamic measurements [S14]). The FM contribution reaches nearly 100% at low T. In contrast, for $x = 11\%$, a broad field distribution ($R = 0.8$ used for all T) is required to describe the increased inhomogeneities close to x_c; and the effective distribution width Δ does not vanish at T_c. Even at the lowest temperatures, the FM contribution does not reach 100%, instead about 20% of $A(t)$ remains paramagnetic. In both compounds the FM contribution is essentially static at low T (fluctuation rate $\nu < 0.2\mu s^{-1}$); it becomes more dynamic towards T_c. The decay rate λ of the PM component increases towards the phase transition indicating that it is sensitive towards the magnetic fluctuations of the Ni spins and clusters.

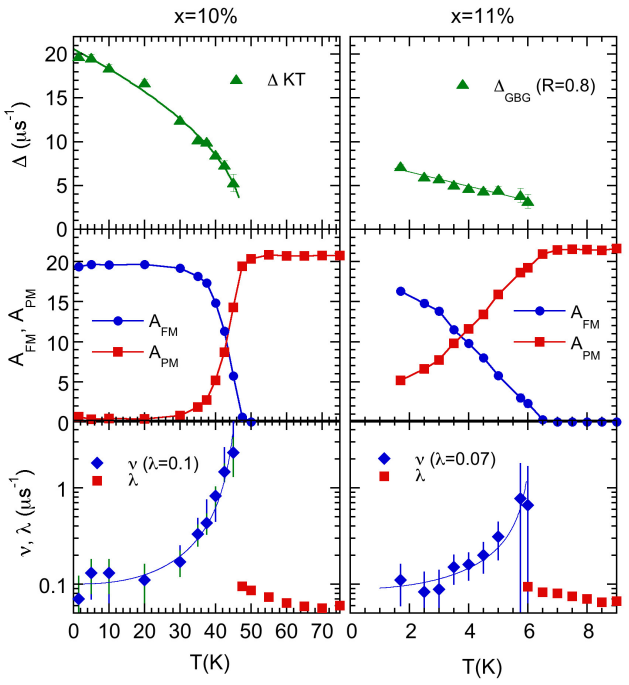

FIG. S4. Temperature dependence of the parameters in μSR analysis for $x = 10\%$ (left) and $x = 11\%$ (right). Top row: KT distribution width Δ for $x = 10\%$ and effective GBG width $\Delta = \Delta_{GBG}$ for $x = 11\%$. Middle row: ferromagnetic and paramagnetic amplitudes A_{FM} and A_{PM}. Bottom row: fluctuation rate ν in the FM phase and depolarization rate λ of the PM phase.

We note in passing that the behavior of the $x = 11\%$ sample close to T_c can also be described by a stretched exponential form $\exp(-(\lambda t)^\beta)$ with $\beta \approx 0.5$. Such behavior is often found for spin glasses [S15] or in non-Fermi liquid compounds [S16] and implies multiple time scales and/or spatial correlations. At lower temperatures ($T < T_c$), a single stretched exponential form cannot account for the short and long time depolarization. The very different depolarization rates are better represented by a two-component model (S1).

Our analysis of the μSR data thus demonstrates that the $x = 11\%$ sample features strongly inhomogeneous static ferromagnetic order coexisting with fluctuating magnetic clusters.

* Present address: Sonoma State University, Department of Engineering Science, Rohnert Park, CA 94928

† Present address: Durham University, Centre for Materials Physics, South Road, Durham DH1 3LE, UK

‡ Present address: Neutron Scattering and Magnetism, Laboratory for Solid State Physics, ETH Zürich, CH-8093 Zürich, CH

[S1] S. Ubaid-Kassis, T. Vojta, and A. Schroeder, Phys. Rev. Lett. **104**, 066402 (2010).

[S2] A. Schroeder, R. Wang, P. J. Baker, F. L. Pratt, S. J. Blundell, T. Lancaster, I. Franke, and J. S. Möller, J. Phys. Conf. Series **551**, 012003 (2014).

[S3] A. Gebretsadik, R. Wang, A. Schroeder, and K. Page, To be published.

[S4] T. Proffen, T. Egami, S. Billinge, A. Cheetham, D. Louca, and J. Parise, Appl. Phys. A **74**, s163 (2002).

[S5] J. Neuefeind, M. Feygenson, J. Carruth, R. Hoffmann, and K. K. Chipley, Nuclear Instruments and Methods in Physics Research B **287**, 68 (2012).

[S6] T. Proffen and S. J. L. Billinge, J. Appl. Crystallogr. **32**, 572 (1999); C. L. Farrow, P. Juhas, J. W. Liu, D. Bryndin, E. S. Bozin, J. Bloch, T. Proffen, and S. J. L. Billinge, J. Phys. Condens. Matter **19**, 335219 (2007).

[S7] T. Proffen, V. Petkov, S. J. L. Billinge, and T. Vogt, Zeitschrift für Kristallographie - Crystalline Materials **217**, 47 (2009).

[S8] J. Liu, A. Huq, Z. Moorhead-Rosenberg, A. Manthiram, and K. Page, Chemistry of Materials **28**, 6817 (2016).

[S9] R. S. Hayano, Y. J. Uemura, J. Imazato, N. Nishida, T. Yamazaki, and R. Kubo, Phys. Rev. B **20**, 850 (1979).

[S10] E. Kornilov and V. Pomjakushin, Physics Letters A **153**, 364 (1991).

[S11] A. Yaouanc and P. Dalmas de Reotier, *Muon Spin Rotation, Relaxation, and Resonance: Applications to Condensed Matter* (Oxford University Press, Oxford, 2011).

[S12] F. Pratt, Physica B **289-290**, 710 (2000).

[S13] D. R. Noakes and G. M. Kalvius, Phys. Rev. B **56**, 2352 (1997).

[S14] R. Wang, S. Ubaid-Kassis, A. Schroeder, P. Baker, F. Pratt, S. Blundell, T. Lancaster, I. Franke, J. Möller, and T. Vojta, J. Phys. Conf. Series **592**, 012089 (2015).

[S15] Y. J. Uemura, T. Yamazaki, D. R. Harshman, M. Senba, and E. J. Ansaldo, Phys. Rev. B **31**, 546 (1985).

[S16] D. E. MacLaughlin, R. H. Heffner, O. O. Bernal, K. Ishida, J. E. Sonier, G. J. Nieuwenhuys, M. B. Maple, and G. R. Stewart, J. Phys. Condens. Matter **16**, S4479 (2004).